A New MEMS Sensor for AC Electric Current

Eli S. Leland, Christopher T. Sherman, Peter Minor
Department of Mechanical Engineering
University of California, Berkeley
Berkeley, California 94720
{esleland | ctsherman | pminor}@berkeley.edu

Richard M. White
Berkeley Sensor and Actuator Center
Department of Electrical Engineering and Computer Sciences
University of California, Berkeley
Berkeley, California 94720

Paul K. Wright
Center for Information Technology Research in the Interest of Society
Department of Mechanical Engineering
University of California, Berkeley
Berkeley, California 94720

***Abstract*—This paper presents new results in the testing and characterization of a MEMS sensor for AC electric current. The sensor is comprised of a piezoelectric MEMS cantilever with a microscale permanent magnet mounted to its free end. When placed near a wire carrying AC current the magnet couples to the oscillating magnetic field around the wire, deflecting the cantilever and generating a sinusoidal voltage proportional to the current. Unlike inductive sensors, this sensor does not need to encircle the conductor and it can measure current in a two-wire "zip-cord". It is also self-powered, and is thus more suitable for wireless sensor node applications than a powered sensor device. The theoretical basis of this new sensor's operation is presented, as well as the fabrication of a MEMS sensor device, and the first test results of this new sensor measuring current in single-wire and two-wire conductors. Sensor response is linear ($R^2 > 0.99$) with sensitivity in the range of 0.1-1.1 mV/A. An integrated self-powered sensor device is also presented, which employs a piezoelectric energy harvester to power the sensor's signal conditioning circuitry at a 2.6% duty cycle.**

I. Introduction

The "smart grid", energy efficiency, and improved reliability of the electric power distribution infrastructure will all depend upon sensor technologies that measure electricity use in homes, businesses, and electric power networks. Advances in the field of micro-electro-mechanical systems (MEMS) can now provide a new class of low-cost, highly-reliable sensors. Developments in low-power radios also enable the deployment of ubiquitous networks of wireless sensors [1] that can monitor and measure the physical world. Research continues into powering wireless sensor devices using energy scavenged from the environment [2]. Combined, these trends provide motivation for the development of a new type of MEMS sensor to measure AC electric current.

The MEMS sensor for AC electric current is comprised of a piezoelectric aluminum nitride (AlN) MEMS cantilever with a microscale composite permanent magnet (micromagnet) mounted on the cantilever's free end (Fig. 1). When placed in proximity to a wire carrying AC current, the alternating magnetic field surrounding the wire induces a sinusoidal force on the sensor magnet, deflecting the piezoelectric cantilever and thus producing a voltage signal proportional to the current in the wire. Unlike existing integratable current sensing technologies [3], this sensor is passive, requiring no power source, and will thus not constitute a drain on the limited energy budget of a wireless sensor node. In addition, it need only be placed in proximity to a conductor in order to measure its current, and it can measure currents in two-wire "zip-cords" without separating the two conductors, unlike alternative technologies such as Rogowski coils and current transformers.

This paper presents the theoretical basis of this sensor design, as well as the fabrication process for a MEMS current sensor prototype. Experimental results evaluating the performance of the MEMS current sensor are presented, as is the demonstration of an integrated device employing a piezoelectric energy harvester to power the sensor's signal conditioning circuitry.

II. Theoretical Background and Design Considerations

The theoretical model describing the behavior of this new current sensor design comprises two major components: the

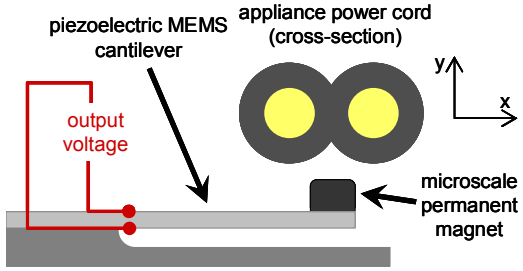

Figure 1. Schematic of the MEMS AC current sensor (not to scale).

This research was sponsored by the California Energy Commission through contract 500-01-43.

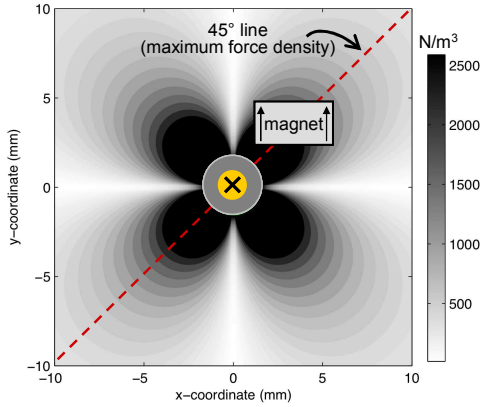

Figure 2. *y*-directed force density surrounding a single wire, 1 A current. Darker shades indicate regions of greater force density. (Assumes *y*-directed magnetization, magnet remanence $B_r = 0.4$ T.)

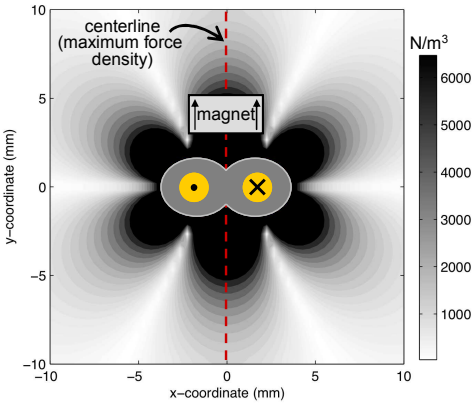

Figure 3. *y*-directed force density surrounding a 16 AWG zip-cord, 1 A current. Darker shades indicate regions of greater force density. (Assumes *y*-directed magnetization, magnet remanence $B_r = 0.4$ T.)

force on a permanent magnet near an AC current-carrying wire and the voltage developed in a piezoelectric cantilever as a result of force applied to its tip. This section presents a high-level overview of this model. A detailed derivation of this model, along with experimental validation, is presented in [4].

A. Force on a Permanent Magnet near an AC Current-Carrying Wire

The force on a permanent magnet in a magnetic field is proportional to the integral of the magnetic field gradient over the magnet's volume [5]. Considering the case of a magnet near a long current-carrying wire (Fig. 1), the forces on the magnet in the plane normal to the wire are described by (1).

$$F_x = B_r \int \frac{d}{dx}\left(H_y\right) dV\,, \quad F_y = B_r \int \frac{d}{dy}\left(H_y\right) dV \tag{1}$$

In these equations, x and y are the horizontal and vertical directions, respectively (Fig. 1), F is the force on the magnet, H_x and H_y are horizontal and vertical components of the magnetic field in amperes per meter, B_r is the remanence of the permanent magnet in Tesla, and V is the magnet's volume. We assume that the remanence of the permanent magnet is uniform and aligned in the positive *y*-direction.

An analysis of the gradient of the magnetic field surrounding a wire begins by recalling the field surrounding a single current-carrying wire is described by (2).

$$\vec{H} = \frac{i}{2\pi r} \tag{2}$$

H is the magnetic field (A/m), i the current in the wire (A), and r the radial distance from the wire to the point of interest. The direction of H is determined using the "right hand rule," aligning the thumb of the right hand with the direction of the flowing current. As force on the sensor magnet is proportional to its remanence B_r (1), once the remanence and magnetization of the sensor magnet are assumed, the "force density" field (with units of N/m^3) surrounding a current-carrying wire can be plotted.

Fig. 2 displays the *y*-directed force density field surrounding a single wire. The contours of this plot trace absolute values of the gradient, because the wire carries AC current and really it is the magnitude of the force generated on the magnet that is of primary concern. Darker regions of Fig. 2 indicate greater force density. The plot shows that the sensor design presented in this paper will develop maximum response when the sensor's magnet is placed as near to the wire as is feasible, and when the magnet is oriented such that its magnetization vector makes a 45° angle with its radial vector to the center of the wire. This orientation corresponds to the dashed diagonal line drawn on the plot, though orientation along a diagonal line cutting from top-left to bottom-right on the plot (not shown) would be equally advantageous.

As the intended application of this research is to monitor residential and commercial electricity use, we examine the case of a two-wire zip-cord common to many appliances. The gradient of the magnetic field surrounding a zip-cord is calculated by superimposing the magnetic fields from each of the two parallel wires and calculating the gradient, and the force density field can be plotted as described above. Fig. 3 shows the *y*-directed magnetic force density surrounding a zip-cord, with darker shades indicating regions of greater force density. Magnet placement along the vertical dashed line that bisects the appliance cord's cross section in Fig. 3 is particularly advantageous. It corresponds to a region where significant force is developed and it has the added benefit that any horizontal forces are balanced due to symmetry.

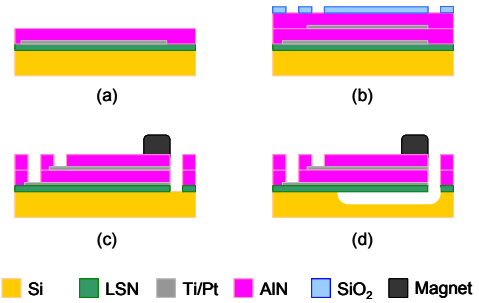

Figure 4. Four-mask cleanroom fabrication process for the MEMS AC current sensor.

B. *Voltage Developed in a Piezoelectric Cantilever as a Result of Tip Deflection*

Roundy and Wright developed an analytical model for the power output of a piezoelectric cantilever when used for vibration energy harvesting [2]. Using their method of analysis produces state equations (3), which describe the relationship between strain, voltage, and input force on a piezoelectric cantilever.

$$\ddot{S} + 2\zeta_m \omega_n \dot{S} + \omega_n^2 S = \frac{k_{sp} a_1 d_{31}}{m t_p} V + \frac{F_{in}}{k_2 m}$$
$$\dot{V} = \frac{a_3 c_p d_{31} t_p}{a_2 \varepsilon} \dot{S} \quad (3)$$

In these state equations S is the strain developed in the cantilever's piezoelectric layer(s) due to tip deflection, V is the voltage developed across the piezoelectric layer's electrodes and F_{in} is the sinusoidal force on the tip-mounted sensor magnet. Continuing, m is the mass of the sensor magnet, k_{sp} is the equivalent spring constant of the cantilever's tip deflection, k_2 is a geometric term relating tip displacement to average strain in the piezoelectric layer, ω_n is the natural frequency of the equivalent spring-mass system and ζ_m is the dimensionless mechanical damping coefficient of the cantilever. The thickness of the piezoelectric layer appears as t_p, c_p is the elastic modulus of the piezoelectric material, d_{31} is the piezoelectric coupling coefficient, and ε is the dielectric permittivity of the piezoelectric material. Finally, a_1, a_2 and a_3 are constants determined by whether the piezoelectric cantilever is a unimorph, a series-poled bimorph, or a parallel-poled bimorph [4].

Equations (3) can be solved using Laplace analysis to produce the frequency response function shown in (4). This equation describes the frequency and magnitude of the piezoelectric cantilever's open-circuit voltage signal in response to the sinusoidal force on the tip magnet when placed near an AC current carrier.

$$V_{oc} = F_{in} \frac{c_p d_{31} t_p a_3}{\varepsilon k_2 m a_2} \frac{1}{\omega_n^2 \left(1 - \frac{c_p d_{31}}{\varepsilon}\right) - \omega^2 - j(2\zeta_m \omega_n \omega)} \quad (4)$$

In this equation F_{in} becomes the amplitude of the sinusoidal force on the tip-mounted sensor magnet, ω is its angular frequency in radians/second (note that mains current is generally 60 Hz in North America and 50 Hz in Europe), and j is the imaginary number ($\sqrt{-1}$).

III. MEMS Device Fabrication

Aluminum nitride (AlN) was chosen as the active piezoelectric material because of its desirable properties for sensor applications [6] and CMOS-compatibility. Released AlN cantilevers were fabricated using a four-mask process in the microfabrication facility at the University of California, Berkeley. Beginning with an Si wafer, 300 nm of insulating low-stress nitride (LSN) was deposited by LPCVD, followed by a 10 nm Ti electrode seed layer and a 200 nm Pt electrode deposited by electron beam evaporation and liftoff patterning, and further followed by a sputter-deposited 1.4 μm AlN active layer (Fig. 4a). A second Ti/Pt electrode was deposited, followed by a second "passive" AlN layer, and a patterned SiO_2 "hard mask" (Fig. 4b). A Cl_2 plasma etch opened vias to the electrodes and defined a U-shaped etch trench around the unreleased cantilever structure, after which the wafer was diced and micromagnets were deposited as described below (Fig. 4c). The sensor cantilevers were released from the substrate using a gaseous XeF_2 etch (Fig. 4d).

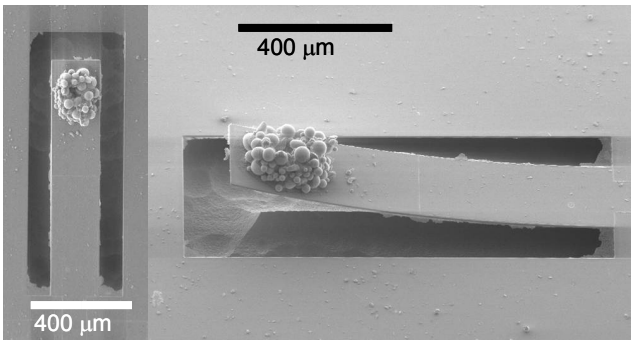

Figure 5. A MEMS AC current sensor measuring 1000 μm × 200 μm, electroded along half its length.

A direct-write dispenser printer [7] was used to fabricate microscale permanent magnets using Magnequench SQP S-11-9 neodymium alloy magnetic powder and a Hexion EPON 828 epoxy binder. The dispenser printer is comprised of a pneumatic pressure controller connected to a syringe that can dispense finely-controlled droplets of functional "ink" onto a substrate. A "dot" of uncured epoxy mixture approximately 150 μm in diameter was first printed on the cantilever tip. Magnetic powder was then manually dispersed over the MEMS die with a small spatula, adhering the particles to the substrate only where epoxy had been printed. The epoxy was cured for several hours at room temperature, whereupon the excess magnetic powder was removed, resulting in a small cluster of magnetic particles firmly adhered to the cantilever tip. This process was repeated three times for each magnet, augmenting the magnet's height with each iteration. A final layer of epoxy was printed on top of the magnet structure in order to provide additional mechanical stability. The micromagnets were magnetized in a 4 T field using a Quantum Design Physical Property Measurement System. This method produced micromagnets approximately 150 μm in diameter and 100 μm tall. An SEM of a released AlN cantilever with a printed composite micromagnet is shown in Fig. 2. Magnetic properties of the micromagnets were characterized using a Quantum Design MPMSXL-7 vibrating sample magnetometer. Magnetic remanence (B_r) of the sensor magnets was found to be approximately 0.4 T, comparing well to values for micromagnets found in the literature [8]. Fig. 5 shows an SEM image of a current sensor prototype.

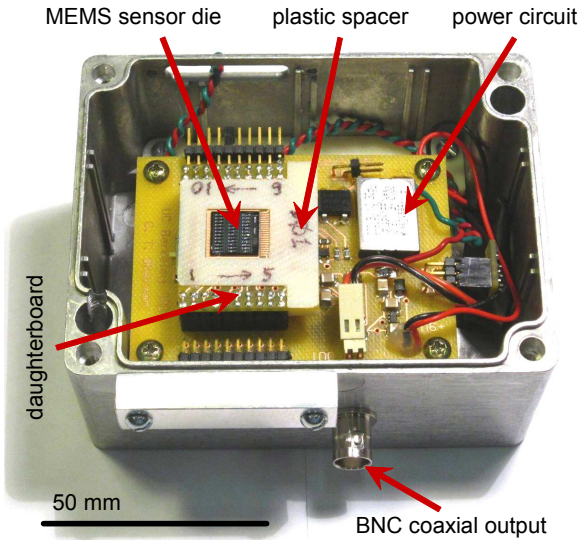

Figure 6. MEMS AC current sensor and enclosure assembly.

IV. Sensor Packaging and Test Apparatus

The sensor die was mounted to a custom-fabricated "daughterboard" configured with 10 pairs of wirebond pads, allowing electrical connection to an equal number of MEMS sensor devices from each die. A thin plastic spacer was placed around the sensor die for mechanical protection. A rectangular window in the spacer accommodated the sensor die and daughterboard bond pads. This daughterboard was connected using pin headers to a motherboard containing signal conditioning and power circuitry. The sensor signal was amplified using a Texas Instruments INA322 instrumentation amplifier, chosen for its high sensitivity and low power consumption. The amplifier circuit was designed to allow switch-selected gain ratios of 10, 50, 100, and 500. The "active" sensor was chosen from among the 10 devices wirebonded to each daughterboard using jumper switches.

A custom circuit provided power to the amplifier, using either a battery or a piezoelectric energy harvester as the power source. Positive and negative supply voltages were provided to the amplifier using a Microchip Technologies MCP1801T regulator and a Maxim MAX828 inverter, respectively. During battery operation these components were powered directly by a rechargeable 9 V battery.

For energy harvesting operation, a piezoelectric energy harvester was constructed from a Piezo Systems Q220-A4-203YB pre-mounted PZT bimorph cantilever with several small neodymium alloy magnets mounted to the cantilever's free end. The position and quantity of the magnets was adjusted to tune the harvester's resonance frequency to 60 Hz in order to maximize coupling and thus power output. The operating principle behind this energy harvester is identical to that of the MEMS current sensor, however the harvesting device is designed to produce usable electrical power rather than a measurement signal. The harvester's output was rectified using a DF005M rectifier and used to charge a 10 mF supercapacitor. The charge state of the capacitor was monitored using a Maxim MAX6433 battery monitor. The

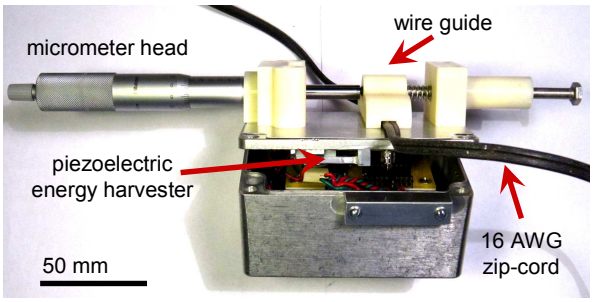

Figure 7. MEMS current sensor enclosure and wire positioning apparatus. Enclosure lid is held slightly ajar for the purposes of this illustration.

capacitor was allowed to charge to 4.99 V, at which point its stored energy was used to power the amplifier circuitry. Once the capacitor drained to 4.36 V, the battery monitor cut off power to the amplifier and the capacitor began charging again. This energy harvesting power source allowed the integrated sensor device to operate intermittently without a battery.

The mounted sensor die and all associated circuitry were placed inside a Velleman G113 aluminum enclosure measuring 115 mm × 90 mm × 55 mm. A window was cut in the lid of the enclosure to allow the sensor die to sit as near as possible to the enclosure's top surface. The energy harvester was mounted to the underside of the enclosure lid, with a second window cut to accommodate the harvester's magnets. A piece of 400 μm-thick aluminum shim stock was placed over the top of the enclosure to protect the MEMS sensor die and to ensure isolation from electromagnetic interference.

A custom-fabricated wire positioning system was mounted to the top of the sensor enclosure in order to provide precise positioning of the AC current-carrying wire to the MEMS sensor and the energy harvester. A Mitutoyo micrometer head provided up to 40 mm of travel, while a plastic wire guide held the wire flat against the top surface of the enclosure. Figs. 6 and 7 show the sensor enclosure assembly described herein.

V. Experimental Results

A. MEMS AC Current Sensor Performance

Two different sensor configurations were used to measure electric current in the four different types of wires: 16 AWG (American Wire Gauge) and 18 AWG zip-cords, and 10 AWG and 14 AWG single wires, where lower gauge corresponds to greater conductor diameter (Table I). The first sensor tested measured 1000 μm × 200 μm and was electroded along its entire length. Its measured resonance frequency was 1.23 kHz. The second sensor had the same dimensions but was electroded along half its length. Its measured resonance frequency was 960 Hz. Variability in the micromagnet fabrication process produced a larger and heavier magnet on this second sensor, resulting in a lower resonance frequency.

A variable transformer was used to supply currents in the range of zero to 25 A_{RMS} in each of the four types of wire, and the amplified sensor signal was acquired using a National Instruments data acquisition card. The sensor's output was amplified by a factor of 100, and during these tests a 9 V battery powered the amplifier circuitry. In each test the

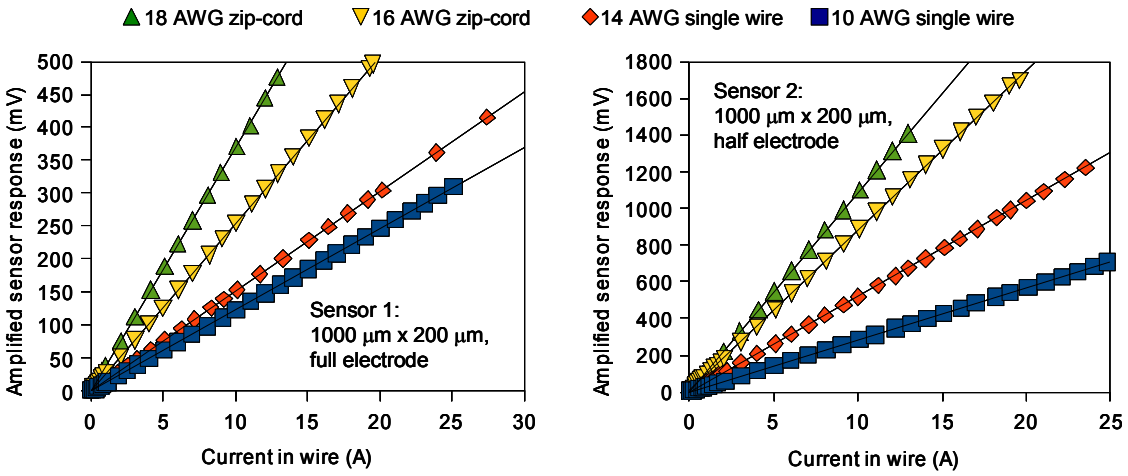

Figure 8. Response of two sensor configurations measuring current in four different types of wire. Plots display amplified response, gain ratio of 100. Currents and voltages shown are RMS values.

positioning system was used to find the wire location resulting in maximum sensor response, and data were taken with the wire held in that position. Fig. 8 plots the results of this experiment. The "raw" unamplified sensitivities are further tabulated in Table 1.

TABLE I. UNAMPLIFIED MEMS CURRENT SENSOR RESPONSE

Number of Conductors	AWG	Conductor Diameter (mm)	Sensor 1 Sensitivity (mV_{RMS}/A_{RMS})	Sensor 2 Sensitivity (mV_{RMS}/A_{RMS})
1	10	2.59	0.122	0.281
1	14	1.63	0.150	0.527
2	16	1.29	0.253	0.870
2	18	1.02	0.365	1.08

The higher-gauge wires have a smaller conductor diameter and thus allow the sensor to be positioned closer to the conductors, resulting in greater sensitivity. The sensor had greater sensitivity measuring currents in the zip-cords both because the conductors were of smaller diameter than those in the single wires, and because in the case of a zip-cord there are twice as many conductors carrying equal currents, each contributing to the force on the sensor magnet.

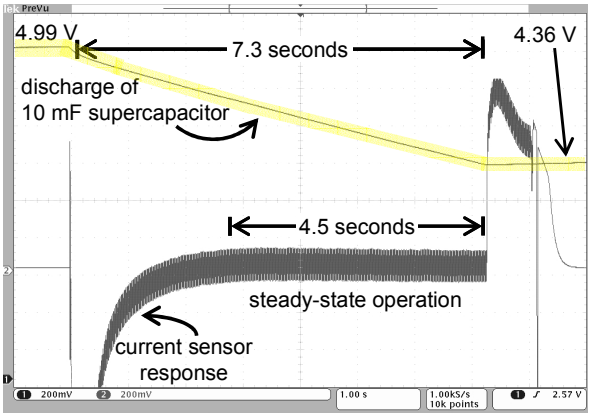

Figure 9. Oscilloscope screenshot during energy harvesting-powered operation. Upper trace (highlighted) shows the discharge of the storage capacitor, lower trace shows the amplified signal from the current sensor.

The force exerted on the tip of the cantilever by the sensor magnet is proportional to the magnet's volume, so a larger sensor magnet generates greater force and leads to greater sensitivity. This partially explains why the sensitivities of the second sensor exceed those of the first by a factor of 2.3-3.5. The second cause for the greater sensitivity of the second sensor is the difference in electrode configurations. Piezoelectric voltage, and thus sensitivity, is related to the average strain under the electrode [4]. Strain is greatest near the base of the sensor cantilever and zero at its tip. The second sensor, on which the electrode extends along only half its length, develops greater average strain under the electrode and is thus more sensitive. As of this writing work continues to evaluate the performance of a wider variety of MEMS current sensor sizes and electrode configurations.

B. Energy Harvesting-Powered Sensor Operation

The sensor was configured using the energy harvesting power source and coupled to a 16 AWG zip-cord carrying a 12 A_{RMS} current. This configuration simulated operation of the sensor measuring the current draw of a 1.44 kW household appliance. In this mode, the energy harvester charged the 10 mF supercapacitor from 4.36 V to 4.99 V in 164 seconds, for an average charging rate of 180 µW. Discharge of the capacitor down to 4.36 V took 7.3 seconds, representing an average power draw of 4 mW for the amplifier circuitry. Fig. 9 shows an oscilloscope screenshot capturing both the capacitor's discharge cycle and the amplified output of the MEMS current sensor during this same period. Transient behavior was observed at the beginning and end of the capacitor discharge cycle as the amplifier electronics first initialized and subsequently powered down. However a stable, usable signal was produced for 4.5 seconds of this cycle, resulting in a duty cycle of operation of about 2.6%.

C. Magnetic Force Model Confirmation

The compact form of this MEMS current sensor and the precision afforded by the wire positioning system allowed for experimentation to verify the magnetic force density presented above. Holding current steady at 10 A_{RMS}, the positioning

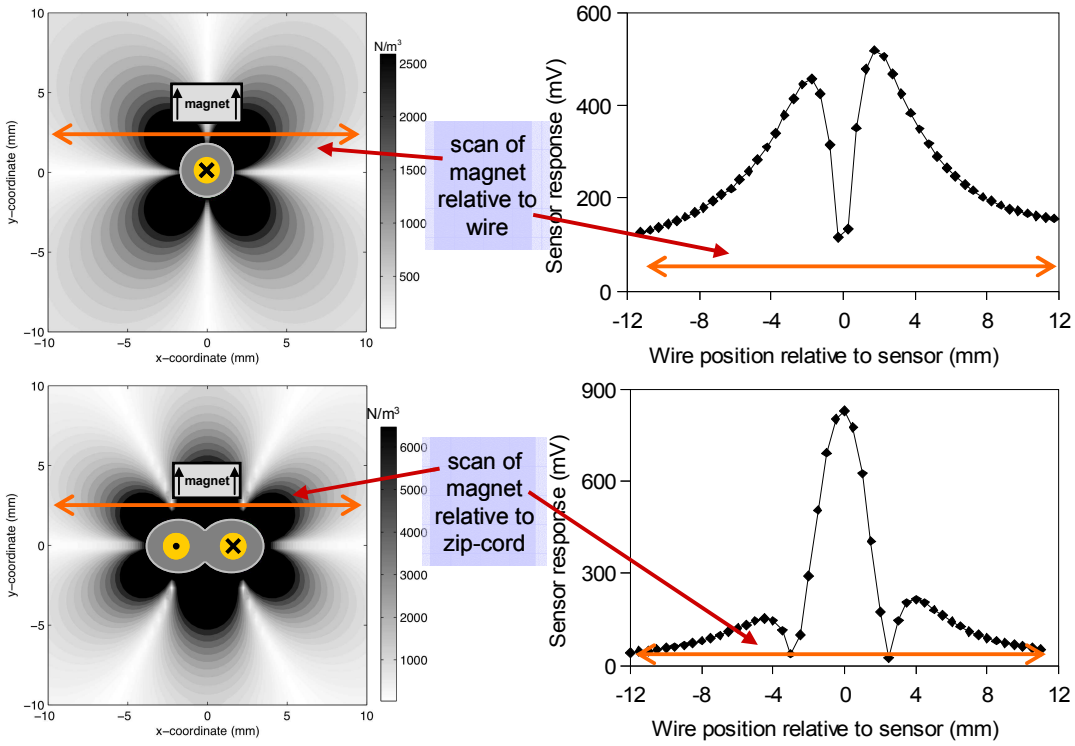

Figure 10. Experimental confirmation of the magnetic force density model presented in Section II. The images on the left are force density plots surrounding a single wire (top) and zip-cord (bottom). Darker shades indicate regions of greater force density. The images on the right display the amplified response of the MEMS current sensor as it is swept through the field surrounding the wire as indicated by the horizontal arrows.

system was used to move both a single wire and a zip-cord past a MEMS current sensor in increments of 0.5 mm, recording the sensor's response at each step. Fig. 10 shows the magnetic force density surrounding a single wire and a zip-cord with the scanning path of the MEMS current sensor superimposed, as well as the response of the sensor as it moved past each wire.

Fig. 10 shows a clear correspondence between the theoretically-derived force density plots and the response of the sensor, further validating the analytical model for magnetic force. The slight lateral asymmetry observed in these plots of sensor response likely resulted from asymmetry of the sensor magnets themselves.

VI. Conclusions and Future Work

- A MEMS sensor for AC current has been fabricated using a piezoelectric aluminum nitride MEMS cantilever with a microscale permanent magnet mounted to its free end. The sensor exhibits linear behavior and is capable of measuring AC current in both single wires and two-wire zip-cords when placed in proximity.
- A self-powered integrated sensor device has been demonstrated, using a piezoelectric energy harvester to power the sensor's signal conditioning circuitry at a 2.6% duty cycle. The potential further exists to incorporate a sensor radio to thus produce a fully self-powered wireless current sensing node.
- Placement of the sensor magnet relative to the current carrier must be chosen carefully to optimize sensor performance. Non-uniformity of micromagnet fabrication will be addressed by incorporating prefabricated microscale block magnets into the sensor design.
- Work continues to further characterize the performance of different sensor dimensions and electrode configurations. Future work will focus on optimizing these parameters to produce the next generation of MEMS AC current sensors.

[1] D. Estrin, et al, "Connecting the physical world with pervasive networks," *Pervasive Computing*, IEEE, 1(1):59–69, Jan-Mar 2002.

[2] S. Roundy and P.K. Wright, "A piezoelectric vibration based generator for wireless electronics," *Smart Mat. & Struct.*, 13(5):1131–1142, 2004.

[3] P. Ripka, "Current sensors using magnetic materials," *J. Optoelectronics and Advanced Materials*, 6(2):587–592, June 2004.

[4] E.S. Leland, "A MEMS Sensor for AC Electric Current," Ph.D. Dissertation, Univ. of California, Berkeley, California, USA, 2009.

[5] B. Wagner, et al., "Permanent magnet micromotors on silicon substrates," *J. Microelectromechanical Systems*, 2(1):23–29, Mar 1993.

[6] S. Trolier-McKinstry and P. Muralt, "Thin film piezoelectrics for MEMS," *J. Electroceramics*, 12(1-2):7–17, 2004.

[7] C.C. Ho, et al, "Direct write dispenser printing of zinc microbatteries," in *Proc. PowerMEMS 2009*, pp. 141-144.

[8] D.P. Arnold and N. Wang, "Permanent Magnets for MEMS," *J. Microelectromechanical Systems*, 18(6):1255-1266, Dec. 2009.